

An Adaptive Finite Element Analysis for Tooth Deformation and Load Distribution of Helical Gears

Yi Zhang, Graduate Student, Department of Mechanical Engineering, The University of Memphis,
yzhang@memphis.edu

Hsiang H. Lin, Professor, Department of Mechanical Engineering, The University of Memphis,
hlin1@memphis.edu

Abstract

An adaptive model of three dimensional finite element approaches has been developed to perform static analysis of helical gears. Several typical contact conditions due to different tooth engagement positions and face widths are studied. Tooth deformation and load distribution along the contact line of separate contact conditions are calculated and compared. For gears with narrower face width or smaller helix angle, local contact compliance has a very significant effect on the total tooth deformation and the load distribution along the contact line is more uniform. On the contact line, the magnitude of tooth load is greater at the points that have higher meshing stiffness and lower deformation. The present model provides more detailed information regarding tooth surface deformation when compared with existing gear literature. It can be used to design helical gears for minimum transmission error to help reduce dynamic loading and stress of the gear systems.

Nomenclature

A_{ij}	sum of displacement at point i of a meshing tooth pair due to an unit load at point j (mm/N)
C_{ij}	displacement of point i on the contact line due to an unit load at point j (mm/N)
E	Young's modulus of elasticity (Mpa)
F	face width of gear tooth (mm)
f_i	displacement of node point i on the contact line (mm)
L_c	contact line length (mm)
M	number of points on the contact line
m_p, m_f	profile and face contact ratios
N_i	interpolation function of node i of an element
P_j	applied load at point j on the contact line (N)
P_{tb}	transverse base pitch (mm)
$R_b, R_p,$	base and pitch radii of gears (mm)
R_t	tip radius of gears (mm)
$[B_i]$	strain shape function matrix
$[D]$	elasticity matrix
$[K_{ij}]$	element stiffness matrix

Greek Symbols

ϕ	normal pressure angle (deg)
μ	Poisson's ratio
ψ_b	helix angle (deg)

Introduction

In comparison with spur gears of the same size, helical gears transmit more load, mesh more smoothly, tend to be quieter, and have less dynamic effects. However, they also have slightly less efficiency and undesirable end thrust during operation. The operating conditions of high precision power transmission have become more severe due to continuous demand for high speed and load. There has been increasing trend on the use of helical gears for power transmission since they can provide greater power, less noise, and longer life than spur gears.

There have been many studies on helical gear transmissions. Nakada and Utagawa [1] derived closed form formula for tooth stiffness of helical gears. Hayashi [2], and Sayama and Hayashi [3] solved numerical integral equations to obtain load distribution. Conry and Seireg [4] developed a mathematical programming algorithm using plate model for evaluating load distribution and optimal modification of gear systems. Umezawa [5-8] investigated the helical gear tooth stiffness with the finite difference method, the approximate formulation method and correlated with the tedious experimental findings. However, there are limited investigations using finite element approach for helical gear analysis. Tobe and Inoue [9] developed a simplified finite element technique by considering the helical gear tooth as a plate. Simon [10], Mathis [11], and Liu [12] used three dimensional finite element method to calculate tooth deflections and load distributions; however, they did not study the contact situations as affected by face width. Li [13] used finite element approach to analyze gear contact with thin rim. Hedlund and Lehtovaara [14] found that gear tooth deformation from finite element analysis can adequately account for the Hertz contact displacement at the mesh locations. Their work mainly dealt with only one face width and load sharing between meshing tooth pairs. Variation of face width can lead to different load distributions and tooth deformations, which will influence the performance of helical gears.

The purpose of this work is to develop an adaptive finite element model to provide accurate analysis of the static behavior of helical gear transmissions under different loading conditions. When the gears rotate, the model will regenerate the finite element mesh of each gear at every contact position to ensure their contact line falls exactly on the node points. This is one of the advantages of developing your own customized finite element model over the use of commercial finite element package. In addition, the contact region of the meshing tooth pair can be further refined for more accurate determination of the tooth contact.

Several typical contact situations of helical gears due to different face widths are to be studied. The effects of those contact conditions on tooth deformation and load distribution are investigated. The present model is evaluated through comparison with the available helical gear data in the literature.

Theory

During the meshing action of a pair of spur gears, the positions of the contact points could be pictured as a series of points moving up the line of action. For helical gears, their contact can be considered as a series of lines moving upwards in the plane of action as shown in Figure 1. Each line makes a helix angle ψ_b with the gear axis and has a vertical spacing between the lines equals to the transverse base pitch P_{tb} . The region of contact is a rectangle of width F (face width) and height ΔS_c (portion of involute tooth profile from the beginning to the end of contact). However, the total contact ratio m_c of a helical gear pair is equal to the sum of profile contact ratio m_p and face contact ratio m_f where

$$m_p = \frac{\Delta S_c}{P_{tb}} \quad \text{and} \quad m_f = \frac{F \tan \psi_b}{P_{tb}} \quad (1)$$

The lines within this region of contact represent the contact lines of a helical gear pair. ΔS_c can be found from the following equation with reference to Figure 2.

$$\Delta S_c = -R_{b1} \tan \phi + \sqrt{(R_{t1}^2 - R_{b1}^2)} - R_{b2} \tan \phi + \sqrt{(R_{t2}^2 - R_{b2}^2)} \quad (2)$$

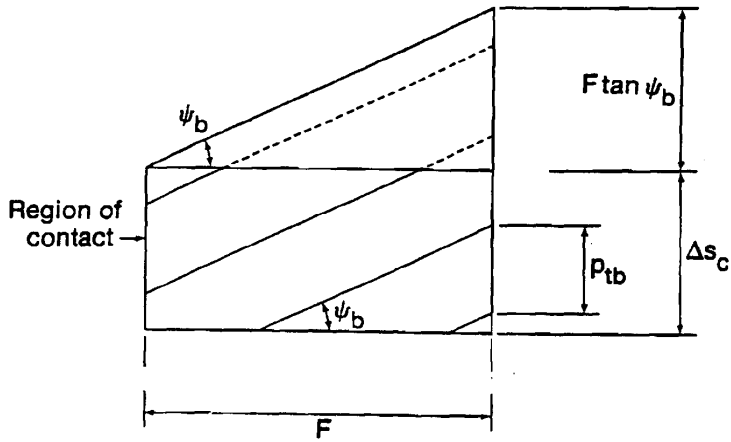


Figure 1 Movement of contact line in the plane of action and along the region of contact

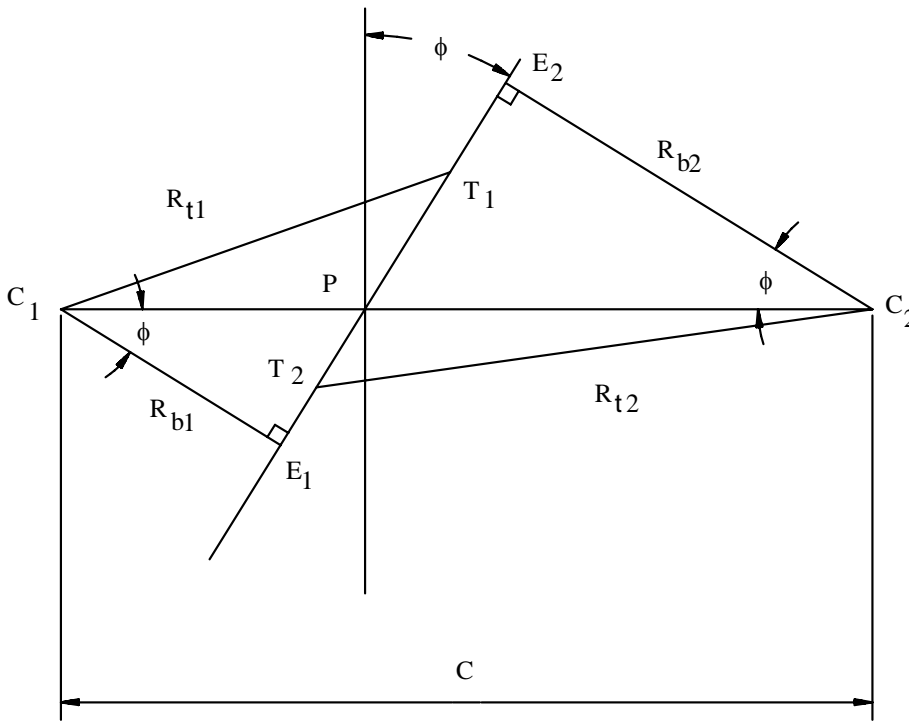


Figure 2 Calculations for the height of the region of contact

Coordinate Transformations

To facilitate the calculations of complicated three-dimensional geometry, several coordinate systems are defined for the mesh of a helical gear pair. First, a local coordinate system, $O_0-X_0Y_0Z_0$ is defined for the tooth end transverse section of helical gears 1 and 2, see Figure 3. Where O_0 is the origin of $X_0Y_0Z_0$ axes, located at the center of the gears, The $X_0Y_0Z_0$ system is so defined that the Y_0 axis passes right through the middle of the end transverse section in radial direction and the Z_0 axis coincides with the gear axis. Also in Figure 3, a second coordinate system $O_1-X_1Y_1Z_1$ is defined with the origin O_1 located at the common pitch

point of the gear pair, the axis Y_1 coincident with the line connecting the center of the gears, and the axis Z_1 parallel to the gear axis.

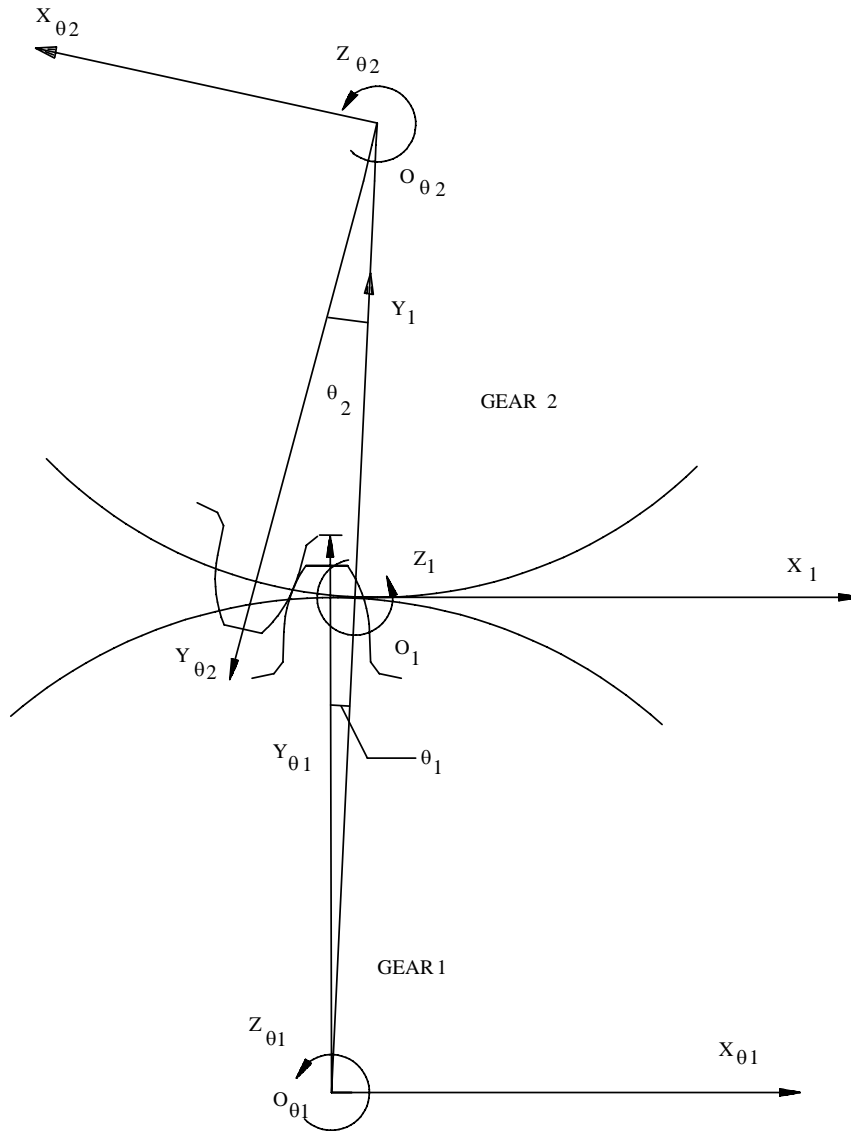


Figure 3 Coordinate systems for helical gears at the gear center and at the common pitch point

The transformation from the first to the second coordinate system can be expressed as follows:

$$\begin{bmatrix} x_1 \\ y_1 \\ z_1 \\ 1 \end{bmatrix} = \begin{bmatrix} \cos \theta_1 & \sin \theta_1 & 0 & 0 \\ -\sin \theta_1 & \cos \theta_1 & 0 & -o_{\theta 1} o_1 \\ 0 & 0 & 1 & -z_{\theta} \\ 0 & 0 & 0 & 1 \end{bmatrix} \begin{bmatrix} x_{\theta 1} \\ y_{\theta 1} \\ z_{\theta 1} \\ 1 \end{bmatrix} \quad (3)$$

$$\begin{bmatrix} x_1 \\ y_1 \\ z_1 \\ 1 \end{bmatrix} = \begin{bmatrix} -\cos\theta_2 & \sin\theta_2 & 0 & 0 \\ -\sin\theta_2 & -\cos\theta_2 & 0 & o_{\theta_2 o_1} \\ 0 & 0 & 1 & -z_\theta \\ 0 & 0 & 0 & 1 \end{bmatrix} \begin{bmatrix} x_{\theta_2} \\ y_{\theta_2} \\ z_{\theta_2} \\ 1 \end{bmatrix} \quad (4)$$

A third coordinate system $O_2-X_2Y_2Z_2$ is defined for the helical gear pair (Figure 4) by rotating the $O_1-X_1Y_1Z_1$ coordinates around the Z_1 axis until the X_2Z_2 plane lies in the plane of action.

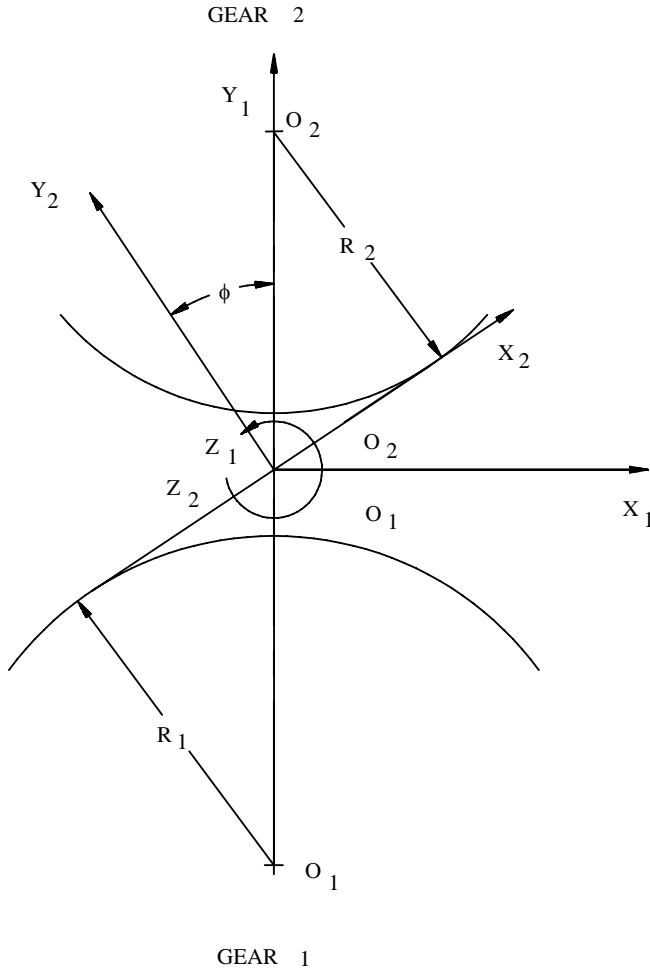


Figure 4 Coordinate systems for helical gears at the common pitch point and along the plane of action

The last coordinate system $O_S-X_SY_SZ_S$ (Figure 5) is achieved by rotating the $O_2-X_2Y_2Z_2$ system around the Y_2 axis so that the X_S axis is in the plane of action and also normal to the tooth surface. The resultant Z_S axis is also in the plane of action but tangent to the tooth surface. This coordinate system contains the contact lines of the gear pair and makes the tooth load calculation very convenient since the transmitted load acts only in the X_S direction.

Y

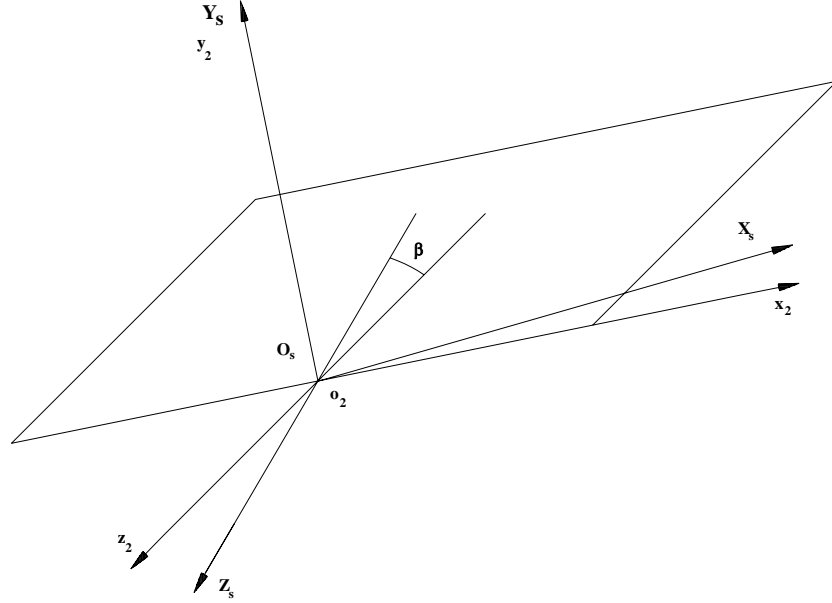


Figure 5 Coordinate systems for helical gears along the plane of action and perpendicular to the tooth surface

Transformations between the above coordinate systems are shown by the following equations:

$$\begin{bmatrix} x_2 \\ y_2 \\ z_2 \end{bmatrix} = \begin{bmatrix} \cos \alpha_t & \sin \alpha_t & 0 \\ \cos \alpha_t & -\sin \alpha_t & 0 \\ 0 & 0 & 1 \end{bmatrix} \begin{bmatrix} x_1 \\ y_1 \\ z_1 \end{bmatrix} \quad (5)$$

$$\begin{bmatrix} X_S \\ Y_S \\ Z_S \end{bmatrix} = \begin{bmatrix} \cos \omega_c & 0 & -\sin \omega_c \\ 0 & 1 & 0 \\ \sin \omega_c & 0 & \cos \omega_c \end{bmatrix} \begin{bmatrix} x_2 \\ y_2 \\ z_2 \end{bmatrix} \quad (6)$$

where $\alpha_t = \arctan(\tan \psi_b / \cos \phi)$, ϕ is the normal pressure angle, ψ_b is the helix angle, and $\omega_c = \arctan(R_{b1}/R_{p1} \tan \psi_b)$, R_{b1} and R_{p1} are base and pitch radii, respectively.

Finite Element Model

After defining the gear geometry and coordinate transformations, a finite element model can be established for a helical gear pair. Eight-node hexahedral isoparametric element with natural coordinate system is used for the model. The stiffness matrix, which relates forces and displacements at the node points of each element, is equal to

$$[k_{ij}] = \iiint [B_i] [D] [B_j] dx dy dz = \int_{-1}^1 \int_{-1}^1 \int_{-1}^1 [B_j] [D] [B_i] J d\xi d\eta d\zeta \quad (7)$$

where [B] is the strain shape function matrix and [D] is the elasticity matrix,

$$[B_i] = \begin{bmatrix} N_{i,x} & 0 & 0 \\ 0 & N_{i,y} & 0 \\ 0 & 0 & N_{i,z} \\ N_{i,y} & N_{i,x} & 0 \\ 0 & N_{i,z} & N_{i,y} \\ N_{i,z} & 0 & N_{i,x} \end{bmatrix} \quad (i = 1, 2, \dots, 8) \quad (8)$$

$$[D] = \frac{E(1-\mu)}{(1+\mu)(1-2\mu)} \begin{bmatrix} 1 & & & & & \\ \frac{\mu}{1-\mu} & 1 & & & & \\ & & \text{symmetric} & & & \\ \frac{\mu}{1-\mu} & \frac{\mu}{1-\mu} & 1 & & & \\ 0 & 0 & 0 & \frac{1-2\mu}{2(1-\mu)} & & \\ 0 & 0 & 0 & 0 & \frac{1-2\mu}{2(1-\mu)} & \\ 0 & 0 & 0 & 0 & 0 & \frac{1-2\mu}{2(1-\mu)} \end{bmatrix} \quad (9)$$

where i is the number of nodes, μ is the Poisson's ratio, E is the Young's modulus of the gear material, and

$$[B_i] [D][B_i]$$

$$= N_{i,x} \begin{bmatrix} N_{i,x} N_{j,x} + A_2(N_{i,y} N_{j,y} + N_{i,z} N_{j,z}) & A_1 N_{i,x} N_{j,y} + A_2 N_{i,y} N_{j,x} \\ A_1 N_{i,y} N_{j,x} + A_2 N_{i,x} N_{j,y} & N_{i,y} N_{j,y} + A_2(N_{i,z} N_{j,z} + N_{i,x} N_{j,x}) \\ A_1 N_{i,z} N_{j,x} + A_2 N_{i,x} N_{j,z} & A_1 N_{i,z} N_{j,y} + A_2 N_{i,y} N_{j,z} \end{bmatrix}$$

$$\left. \begin{array}{l} A_1 N_{i,x} N_{j,z} + A_2 N_{i,z} N_{j,x} \\ A_1 N_{i,y} N_{j,z} + A_2 N_{i,z} N_{j,y} \\ N_{i,z} N_{j,z} + A_2(N_{i,x} N_{j,x} + N_{i,y} N_{j,y}) \end{array} \right] \quad (i = 1, 2, \dots, 8) \quad (10)$$

In the above equation, N_i is the nodal interpolation function of the 8-node element

$$N_i = (1 + \xi_i \xi)(1 + \eta_i \eta)(1 + \zeta_i \zeta) \quad (11)$$

where ξ , η , and ζ represent the natural coordinates, and $N_{i,x}$, $N_{i,y}$, and $N_{i,z}$ are the partial differentiation of N_i with respect to x , y , and z coordinates respectively. Transformation between the natural and rectangular coordinates can be found in many texts that deal with finite element analysis, therefore, will not be repeated here. In the above equation the matrices A_1 , A_2 , and A_3 are

$$A_1 = \mu / (1 - \mu) \quad A_2 = (1 - 2\mu) / [2(1 - \mu)] \quad (12)$$

$$A_3 = E(1 - \mu) / [(1 + \mu)(1 - 2\mu)]$$

Adaptive Mesh Scheme

The portion of the tooth surface that is in contact is discretized with a mesh in such a way that the contact line falls exactly on the node points and that the mesh is finer within the contact region than the non-contact region. Figure 6 shows an example mesh scheme of the tooth surface, where AB represents the contact line. This customized mesh scheme can be more efficient in contact load calculation and is repeated for every contact position of the gear pair throughout the entire tooth mesh cycle. If there are n contact positions in the tooth engagement cycle, there will be n different meshes. The concentrated load of each individual node point on the line will represent the continuous load distribution on the contact line of the meshing gear pair. The system equation of the gear tooth model is developed using basic finite element principles. This customized finite element model can be more efficient than the commercial software and provides easier implementation to model the tooth contact between helical gears.

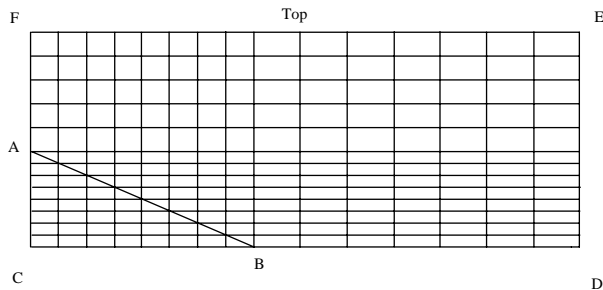


Figure 6 Adaptive finite element mesh for the contact region of a helical gear tooth surface

Boundary Conditions

Figure 7 shows the boundary conditions of a transverse section of the gear tooth model under investigation. At every section the tooth foundation is fixed at the boundary. The size of the tooth foundation, as suggested by Liu [7], has BC arc length equals to three times the normal module and AB equals to one and a half times the normal module.

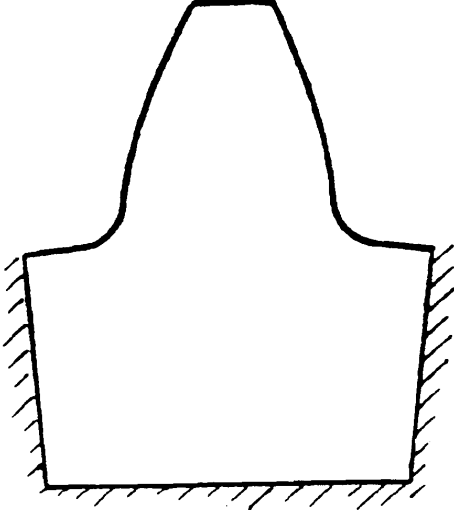


Figure 7 Boundary conditions of the gear tooth model

Tooth Deformation and Load Distribution

The tooth load is assumed to be in the direction normal to the tooth surface. A load in this direction may cause tooth deformations in other directions. However, only the deformation in the load direction will be considered in the study because it is usually significantly greater than those in other directions. To ensure the continuity of tooth contact, the sum of displacements of the meshing teeth at any point on the same contact line must be the same. The displacement of node point i on the contact line can be expressed as:

$$f_i = \sum_{j=1}^M C_{ij} P_j \quad (i = 1, 2, \dots, M) \quad (13)$$

where N is the number of the contact points on the contact line; f_i is the normal displacement of point i ; C_{ij} is the displacement of point i when a unit force is applied at point j ; and P_j is the actual load at point j .

Similar expression can be used for the displacement of the mating gear,

$$f_i' = \sum_{j=1}^M C_{ij}' P_j \quad (i = 1, 2, \dots, M) \quad (14)$$

To maintain continuous contact of the gear teeth, the sum of f_i and f_i' must be the same at every contact point along the contact line. Therefore, for a tooth pair k at any contact point i , we have

$$f_i^k + f_i^{k'} = \sum_{j=1}^M (C_{ij}^k + C_{ij}^{k'}) P_j^k = \sum_{j=1}^M A_{ij}^k P_j^k = C_i^k \quad (i = 1, 2, \dots, M) \quad (15)$$

where A_{ij} is the sum of displacement at point i caused by a unit normal force at point j for a mating tooth pair. If there is more than one tooth pair in contact at the same time, the sum of displacement C of all contacting tooth pairs should be the same.

An iteration method is used to calculate the tooth displacement and load distribution based on the above formulations. To start the iteration, the tooth load is first assumed to be distributed evenly along the contact line. The displacements of contacting tooth pair k (f_i^k and f_i^k) are calculated at each contact point. Apparently, the sum of f_i^k and f_i^k , that is C_i^k , could be different at different contact point before the numerical computation converges. Therefore the average of C_i^k is chosen as the displacement of the meshing tooth pair,

$$C_A = \frac{1}{M} \sum_{i=1}^M C_i^k \quad (16)$$

The load distribution of tooth pair k can be revised by the following equation,

$$P_j^{k,n+1} = P_j^{k,n} \times (1 - (C_j^k - C_A^k) / C_A^k \times Q) \quad (17)$$

where Q is a coefficient to facilitate the convergence of computation. Its value is ranged from 1 to 2. The above steps can be repeated until both the tooth displacement and contact force reach a steady solution.

Results and Discussions

A helical gear pair as listed in Table 1 is chosen for the investigation. The gears are made of carbon steel and modeled with standard gear geometry data.

Table 1 Data of example helical gear pair

Gear Parameter:	Gear 1 (Driving gear)	Gear 2 (Driven gear)
Normal Pressure Angle (deg)	20	20
Helix Angle (deg)	13.54	13.54
Number of Teeth	63	112
Normal Module (mm)	5.08	5.08
Root Diameter (mm)	307.34	556.26
Addendum Diameter (mm)	330.20	579.12
Applied Load (N)	1000	1000

Contact Pattern of Helical Gears

For helical gears their tooth contact can generally be divided into four different contact patterns as shown in Figure 8. Case (a) displays a typical contact situation near the beginning of contact region where the contact line extends from one end of the tooth face to the bottom of working profile. Case (b) depicts the contact near the end of contact region where the contact line goes from the opposite end of the tooth face to the top of the tooth. Cases (c) and (d) demonstrate the possible contact situations in the mid-section of the contact region. For case (c), it has a very wide tooth face and therefore the contact line extends from the tooth tip to the bottom of the working profile. However, for case (d), it has such a narrow face width that its contact line extends from one end of the tooth face to the other. In this study, to illustrate the above contact conditions, the face width for cases (a), (b), and (c) is 130 mm, and that for case (d) is 45 mm. The profile contact ratio m_p is 1.78 and the face contact ratio m_f is 2.03 for cases (a), (b), and (c), and 0.70 for case (d).

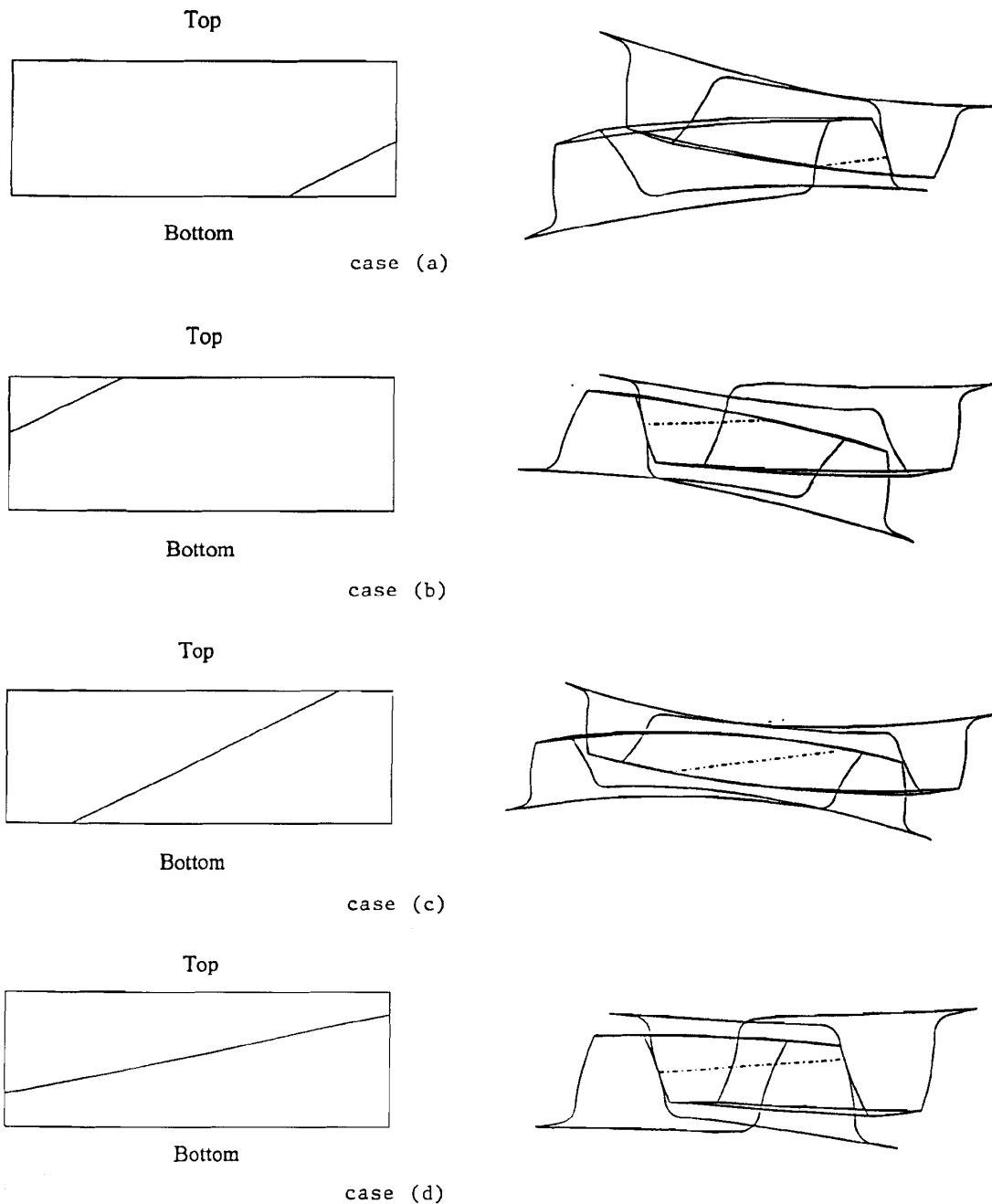


Figure 8 The four different patterns of helical gear tooth contact

Gear Tooth Deformation

Figure 9 shows the three-dimensional deformation of the pinion tooth surface corresponding to the four different contact conditions discussed in Figure 8. The tooth surface deformation should include the effects due to bending, shear, foundation flexibility, and local contact deformation. Comparison of these figures indicates that the local contact compliance has a major influence on the tooth deformation. This is especially more significant for case (d) when the face width is narrower and the load acting on the tooth surface is greater, than the other three cases.

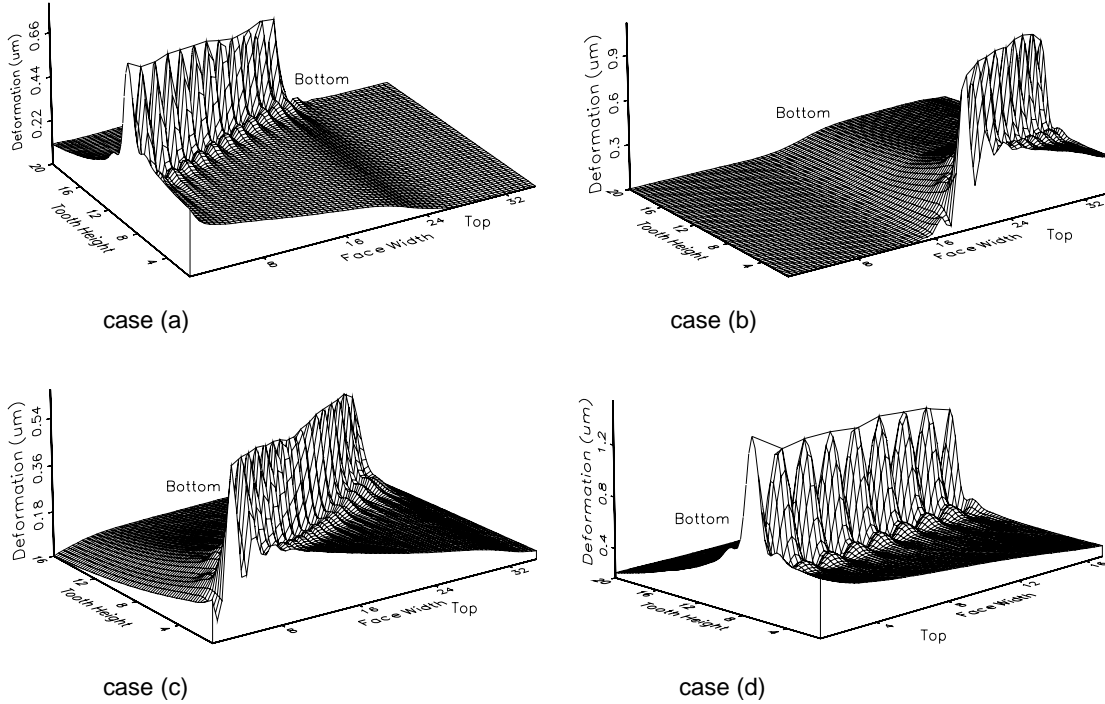


Figure 9 Tooth surface deformations for the four contact patterns of helical gears

Deformations at the tooth ends are higher than those in the middle of the tooth because of weaker support. For cases (a) and (b), the portion of the tooth surface that is outside the contact zone has deformation so insignificant that they are essentially zero. The portion of the tooth within the contact zone has deformations induced by some or all of the deflection components. For cases (c) and (d), where the loading encompasses either the entire length of working depth or face width, tooth deflection along the contact line is more uniform and every part of the tooth surface has some deformation due to this kind of loading.

Tooth Load Distribution

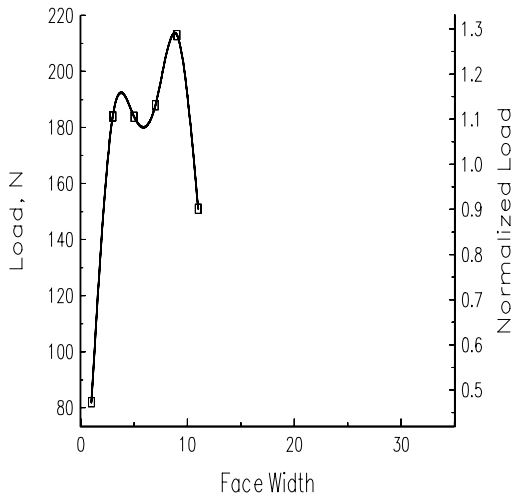
It is essential to evaluate tooth load distribution since it affects the life and performance of helical gears significantly. The portion of tooth face where load is higher would have greater stress and earlier failure. Figure 10 shows the value of concentrated load at each node point on the contact lines for the four cases in Figure 8. In this figure, the abscissa is labeled by the number of transverse section, of finite element model, along the face width rather than by the actual length. Those concentrated loads can be converted into distributed load if divided by a certain length l . For the load at either end of the contact line this length is

$$l = \frac{L_c}{2(M-1)} \quad (18)$$

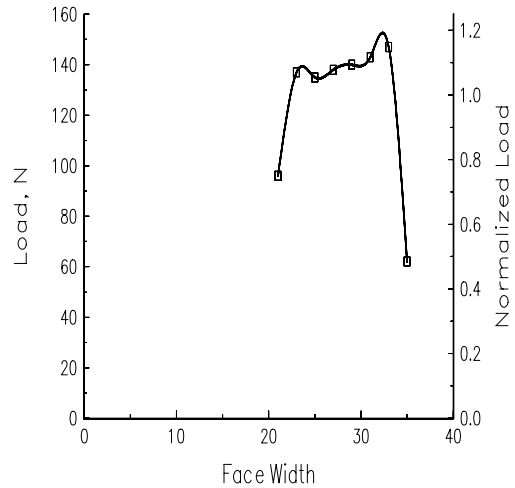
For the load at the rest of the node points on the contact line

$$l = \frac{L_c}{(M-1)} \quad (19)$$

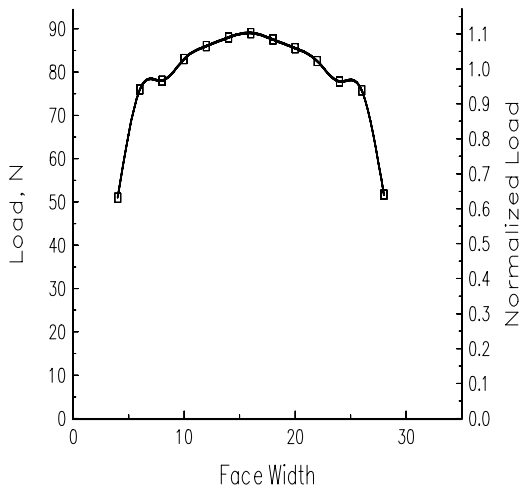
where L_c is the contact line length, M is the number of nodes on the contact line.



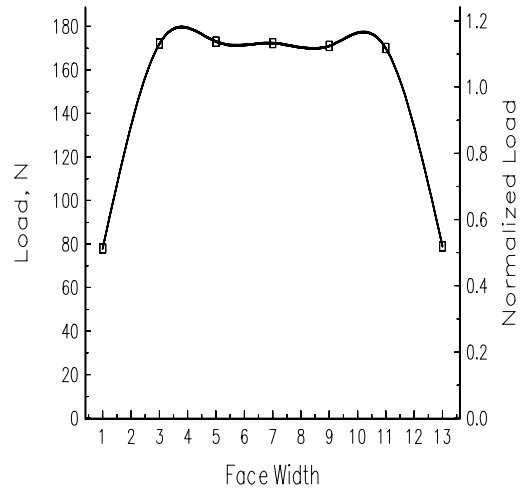
case (a)



case (b)



case (c)



case (d)

Figure 10 Concentrated loads at the node points of the contact lines for the four contact patterns

Figure 11 shows the results of tooth load distribution for the four cases discussed previously. Note that in the figure the load distribution curve for cases (a), (b), and (c) has a peak value at the end point where the top of one tooth is in contact with the root of the mating tooth. This is due to the fact that the tooth meshing stiffness of the gear pair is greater at these end points than at other points on the same contact line. The contact at these end points is more toward the middle of the face width, which provides stronger support. Contrary to the above, for cases (a) and (b) the meshing stiffness of the end points with tooth contact at the edge is lower than those in the middle of the contact line, therefore the distributed load at these end points is smaller. From the concentrated load result, the tooth load distribution for case (d) is much more uniform than the other three cases.

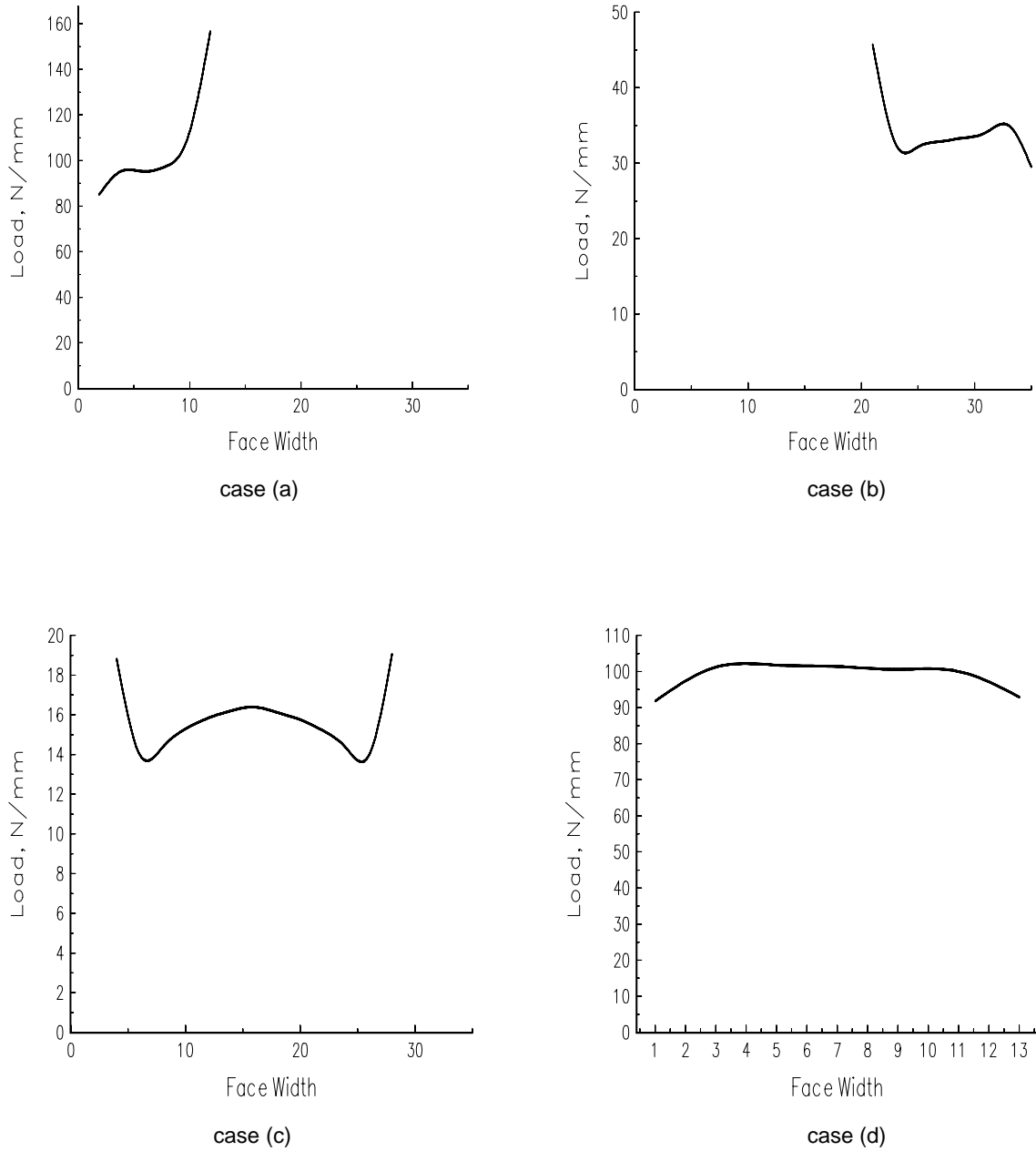


Figure 11 Tooth load distribution along the contact lines for the four contact patterns

The current model needs to be compared with the existing gear literature for evaluation. However, the gear literature available for comparison with the current analysis is very limited. Results presented by several gear researchers [11, 12, 15, 16] were in different contact patterns and with different gear parameters. It is difficult to compare the results of the present study numerically with the existing literature, however, it is feasible to compare the characteristics of current results with that in the literature. The contact pattern of case d has been analyzed more commonly by gear researchers, therefore its result is used for comparison with others. Figure 12 displays the concentrated tooth load data as presented by Mathis [11], Liu [12], and Umezawa [15, 16]. As can be seen from comparing the tooth load results in the figure, the present work has similar characteristics and agrees well with the existing gear literature.

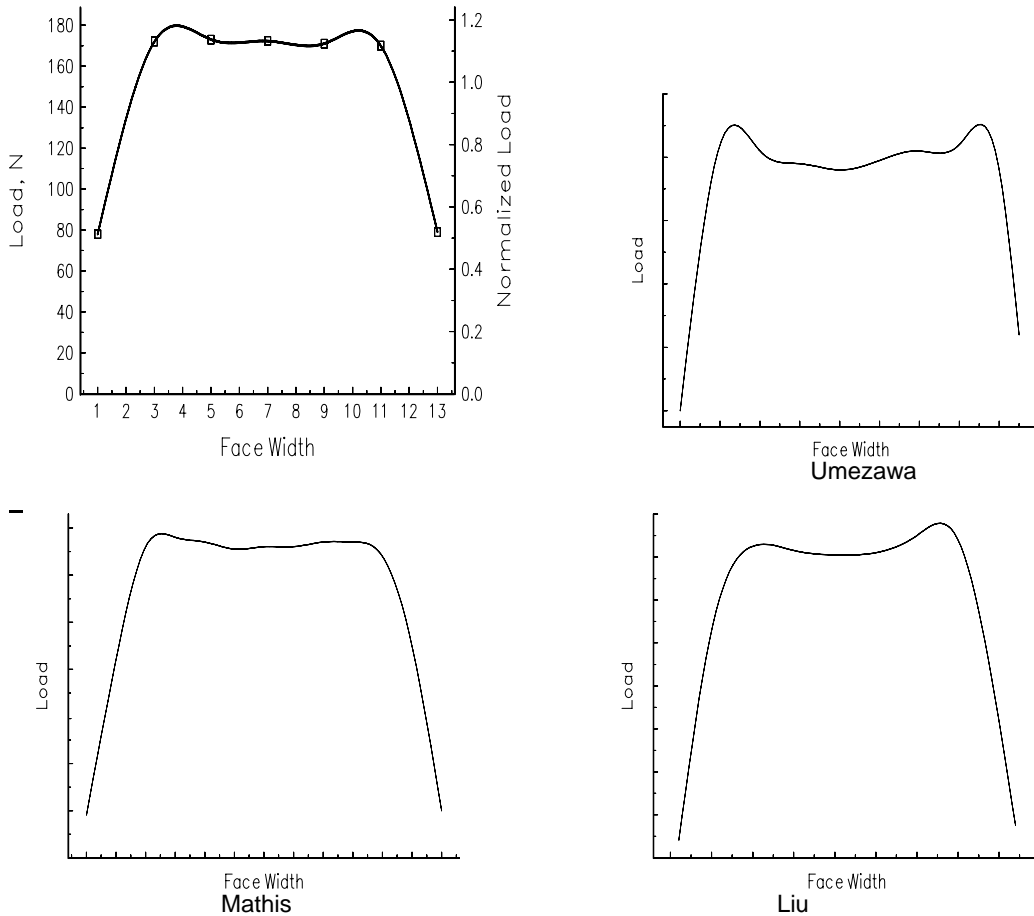


Figure 12 Comparison of the characteristics of concentrated load results with that in the gear literature

Conclusions

A three dimensional finite element program has been developed to investigate the tooth deformation and load distribution of helical gear systems. The program employs adaptive finite element mesh to the contact region to better model the gear tooth engagement. This customized finite element model can be more efficient than the commercial software and provides easier implementation to model the tooth contact between helical gears. Four different tooth engagement conditions are studied to analyze their effects on the tooth deformation and load distribution. Comparison with the limited gear data indicates that the results from the present study are reasonable and agrees well with the existing literature.

The following conclusions can be made based on the results of the current investigation:

1. Local contact compliance has a very significant influence on the tooth deformation especially for gears that have a narrower face width.
2. Tooth deformations at the end of the tooth face are higher than those in the middle of the face width because of weaker support.
3. For a helical gear that have narrow face width the contact line can extend from one end of the tooth face to the other. Such contact condition produces a more uniform load distribution along the contact line.
4. For the load distribution along the contact line, the magnitude of the tooth load is greater at the points that have higher meshing stiffness and lower deformation.

References

1. Nakada, T., and Utagawa, M., "The Dynamic Loads on Gear Caused by the Varying Elasticity of the Mating Teeth," *Proc. Of the 6th Japanese National Congress for Applied Mechanics*, 1956, pp. 43
2. Hayashi, K., "Load Distribution on the Contact Line of Helical Gear Teeth - Part 1", *JSME Bulletin*, Vol. 6, No. 22, 1963, pp. 336 - 343.
3. Sayama, T., and Hayashi, K., "Load Distribution on the Contact Line of Helical Gear Teeth - Part 2", *JSME Bulletin*, Vol. 6, No. 22, 1963, pp. 344 - 353.
4. Conry, T.F., and Seireg, A., "Mathematical Programming Technique for the Evaluation of Load Distribution and Optimal Modifications for Gear Systems", *ASME Journal of Engineering for Industry*, Nov. 1973, pp. 1115 - 1122.
5. Umezawa, K., "The Meshing Test on Helical Gears Under Load transmission", *JSME Bulletin*, Vol. 15, No. 90, 1972, pp. 1632 - 1639.
6. Umezawa, K., and Ishikawa, J., "Deflection due to Contact Between Gear Teeth with Finite Width," *JSME Bulletin*, Vol. 16, No. 97, 1973, pp. 1085 - 1093.
7. Umezawa K., and Ishikawa, J., "On Cylindrical Gears without Statical Behaviors of Driven Gears under Any Load," *JSME Bulletin*, Vol. 18, No. 122, 1975, pp. 897 - 904.
8. Umezawa, K., "The Performance Diagrams for the Vibration of Helical Gears," *ASME 5th International Power Transmission and Gearing Conference*, Chicago, Illinois, Apr. 1989, pp. 399 - 408.
9. Tobe, T., and Inoue, K., "Longitudinal Load Distribution Factor of Helical Gears," *ASME Journal of Mechanisms, Transmissions, and Automation in Design*, Mar. 1985, pp. 17 - 23.
10. Simon, V., "Load and Stress Distributions in Spur and Helical Gears," *ASME Journal of Mechanisms, Transmissions, and Automation in Design*, June 1988, pp. 197 - 202.
11. Mathis, R., "Deformation and Stress of Helical Gears," *Journal of Gear*, Vol. 8, No. 4, 1984, pp. 41 - 45.
12. Liu, S., and Wu, J., "Study on Bending Strength of Involute Helical Gears," *Mechanical Engineering and Technology*, Vol. 1, 1992, pp. 24 - 30.
13. Li, S., "Gear Contact Model and Loaded Tooth Contact Analysis of a Three-Dimensional, Thin-Rimmed Gear," *ASME Journal of Mechanical Design*, Sept. 2002, pp. 511 - 517.
14. Hedlund, J., and Lehtovaara, A., "Modeling of Helical Gear Contact with Tooth Deflection," *Tribology International*, Jan. 2006, pp. 613 - 619.
15. Umezawa, K., and Ishikawa, J., "Deflection Due to Contact Between Gear Teeth with Finite Width", *JSME Bulletin*, Vol. 16, No. 97, July 1973, pp. 1085 - 1093.
16. Umezawa, K., "Recent Trend in Gearing Technology," *JSME Bulletin*, Vol. 31, No. 2, 1988, pp. 357 - 362.